The discovery and characterization of two novel structural motifs on the carboxy-terminal domain of kinetoplastid RNA editing ligases

DANIEL MOSES,[1] VAIBHAV MEHTA,[1,2] and REZA SALAVATI[1,2]

[1]Institute of Parasitology, McGill University, Ste. Anne de Bellevue, H9X 3V9 Quebec, Canada
[2]Department of Biochemistry, McGill University, Montreal, H3G 1Y6 Quebec, Canada

ABSTRACT

Parasitic protozoans of the *Trypanosoma* and *Leishmania* species have a uniquely organized mitochondrial genome, the kinetoplast. Most kinetoplast-transcribed mRNAs are cryptic and encode multiple subunits for the electron transport chain following maturation through a uridine insertion/deletion process called RNA editing. This process is achieved through an enzyme cascade by an RNA editing catalytic complex (RECC), where the final ligation step is catalyzed by the kinetoplastid RNA editing ligases, KREL1 and KREL2. While the amino-terminal domain (NTD) of these proteins is highly conserved with other DNA ligases and mRNA capping enzymes, with five recognizable motifs, the functional role of their diverged carboxy-terminal domain (CTD) has remained elusive. In this manuscript, we assayed recombinant KREL1 in vitro to unveil critical residues from its CTD to be involved in protein–protein interaction and dsRNA ligation activity. Our data show that the α-helix (H)3 of KREL1 CTD interacts with the αH1 of its editosome protein partner KREPA2. Intriguingly, the OB-fold domain and the zinc fingers on KREPA2 do not appear to influence the RNA ligation activity of KREL1. Moreover, a specific KWKE motif on the αH4 of KREL1 CTD is found to be implicated in ligase auto-adenylylation analogous to motif VI in DNA ligases. In summary, we present in the KREL1 CTD a motif VI for auto-adenylylation and a KREPA2 binding motif for RECC integration.

Keywords: trypanosome; RNA editing; ligation; adenylylation; phosphodiester bond formation; carboxy-terminal domain

INTRODUCTION

The kinetoplastid parasites *Trypanosoma brucei*, *Trypanosoma cruzi*, and *Leishmania* spp. cause endemic diseases worldwide, namely human African trypanosomiasis, Chagas disease, and leishmaniases (Stuart et al. 2008; Alalaiwe et al. 2018). These early diverged eukaryotes harbor within their mitochondria, a uniquely organized genome of interlocked dsDNA in the form of mini and maxicircles, known as the kinetoplast (Jensen and Englund 2012). The maxicircles encode several subunits of the electron transport chain and two subunits of the mitochondrial ribosome, while minicircles transcribe short *trans*-acting template guide RNA (gRNA) for use in post-transcriptional maturation of the maxicircle transcripts (Aphasizhev and Aphasizheva 2014; Ramrath et al. 2018). Catalyzed by an ∼800 kDa multiprotein RNA editing catalytic complex (RECC), this process entails insertions and/or deletions of uridine (U) residues to varying degrees in the premature transcripts (Kable et al. 1996; Stuart et al. 2005). Among the catalytic RECC components, the kinetoplastid RNA editing ligase 1 (KREL1) and the kinetoplastid RNA editing protein A2 (KREPA2) are specific for ligation post-U-deletion and are paralogous to KREL2 and KREPA1 that are specific for ligation post-U-insertion (Schnaufer et al. 2003). KREL1 is the essential ligase for parasite survival and functional editing in vivo, while its interacting partner, KREPA2, is critical for RECC stability and KREL1 integration into the complex (Schnaufer et al. 2001; Huang et al. 2002; Guo et al. 2008).

KREL1's ligation mechanism is analogous to the extensively characterized DNA and RNA ligases (Subramanya et al. 1996; Sriskanda and Shuman 1998; Doherty and Suh 2000; Ho et al. 2004; Martins and Shuman 2004). Catalysis can be broken down into three key steps: (i) KREL1 auto-adenylylation, where the ligase catalyzes a covalent linkage between a conserved lysine of motif I with the α-phosphate of ATP to form a KREL1–AMP intermediate while releasing

Corresponding author: reza.salavati@mcgill.ca
Article is online at http://www.rnajournal.org/cgi/doi/10.1261/rna.079431.122. Freely available online through the *RNA* Open Access option.

pyrophosphate; (ii) RNA adenylylation, transfer of AMP to the 5′ PO_4 termini of the nicked RNA duplex; (iii) phosphodiester bond formation, a nucleophilic attack by the 3′ OH group enables the deadenylylated ligase to covalently bind the nicked ends of the RNA while releasing AMP.

Several studies outline the structural domains of KREL1 and KREPA2 and their potential role in the ligation mechanism (Schnaufer et al. 2003; Worthey et al. 2003; Deng et al. 2004; Mehta et al. 2015). The crystallized amino-terminal domain of KREL1 (PDB code 1XDN) reveals the ATP binding site, formed by β-strands containing residues from five key motifs (I, III, IIIa, IV, and V). These functional motifs are highly conserved in nucleotidyl transferase enzymes such as DNA/RNA ligases and mRNA capping enzymes (Supplemental Fig. S1; Subramanya et al. 1996; Deng et al. 2004). Sequence alignments and experimental mutation analysis revealed a conserved sixth motif (VI) in DNA ligases critical for step 1, ligase auto-adenylylation, located outside the binding pocket and in the CTD adjacent to its oligonucleotide binding fold (OB-fold) domain (Sriskanda and Shuman 1998; Samai and Shuman 2012). This motif has been elusive in the KRELs, due to its highly diverged CTD lacking the OB-fold, unlike DNA ligase and mRNA capping enzymes (Ellenberger and Tomkinson 2008; Flynn and Zou 2010). Sequence alignment-based search tools identify bacteriophage T4 RNA ligase 2 (T4Rnl2) as the closest ortholog for the KRELs (Ho and Shuman 2002; Nandakumar et al. 2006). Although the CTD of T4Rnl2 is dispensable in RNA ligation, the deletion of this domain in KREL1 appears detrimental to its activity (Ho et al. 2004; Mehta et al. 2015) implicating a potential motif VI-like region in its CTD. The KREL1 CTD is mainly known for its interaction with KREPA2 as established through yeast-2-hybrid and mutational studies (Schnaufer et al. 2010; Mehta et al. 2015). The current hypothesis for KREPA2's involvement in ligation focuses on its OB-fold domain being provided *in trans* for RNA recognition and binding in a mechanism analogous to the fused OB-fold domain in DNA ligases that interacts with nicked DNA during ligation (Subramanya et al. 1996; Håkansson et al. 1997). While this involvement has not been proven experimentally, the theory has been supported by KREPA2-mediated enhancement of KREL1 activity in vitro (Mehta et al. 2015). Moreover, enhancement of KREL1 auto-adenylylation indicated a likely motif VI also to be provided *in trans*, albeit KREL1 still exhibits robust activity in vitro without its interaction partner.

In this study, we aimed to further characterize the ligation mechanism of kinetoplastid RNA editing ligase. We performed an extensive mutational analysis involving terminal truncations, internal truncations, point mutations and group mutations of the recombinant (r) KREL1 and KREPA2 proteins of *T. brucei*. We narrowed down the KREL1–KREPA2 regions of contact and further tested the effect of this interaction in ligation in vitro. We also identified a diverged motif VI region on KREL1 critical for step 1 activity, ligase auto-adenylylation, which validates the functional role of its CTD. Our results implicate a crucial role for the motif VI in ATP hydrolysis, enhanced by KREPA2 interaction.

RESULTS

KREL1 CTD α-helix 3 interacts with KREPA2 α-helix 1

To narrow the region on KREL1 that interacts with KREPA2, we generated a panel of recombinant KREL1 proteins—full-length and truncated (Fig. 1) and performed pull-down experiments with recombinant KREPA2. We expressed the NTD and CTD of KREL1 independently and showed that its CTD (aa 354–469) can interact with KREPA2 (Fig. 2A), as anticipated from published data (Schnaufer et al. 2010; Mehta et al. 2015). In fact, KREPA2 interaction was completely absent with KREL1 CTD truncates: NTD (aa 51–324) and NTD_VLR (NTD with the variable loop; aa 51–354) (Fig. 2A). We then expressed a series of carboxy-terminal truncations of KREL1 dictated by recognizable conserved regions that structurally resolve into the four α-helices (Fig. 1A; Supplemental Fig. S2). In the KREPA2 pull-down assay, we noticed a loss of binding with the KREL1 384 truncation (aa 51–384) that was subsequently present with the KREL1 410 truncation (aa 51–410) (Fig. 2A), suggesting that the region of KREPA2 contact is between residues 384–410 of KREL1, with the αH3 of its CTD. Hence, we next confirmed the loss of KREPA2 binding with an αH3 internal deletion variant of KREL1 (Δ αH3) (Fig. 2B).

Next, to identify the region on KREPA2 that interacts with KREL1, several versions of rKREPA2 were generated corresponding to the full-length protein, with internal truncations of (Δ)αH1 or the (Δ)OB-fold domain, and mutated ZnFs (Fig. 1B). This experiment shows that KREPA2 Δ OB-fold (aa 1–484) or KREPA2 with cysteine to alanine substitutions in the ZnF domains, have no impact on KREL1 binding activity (Fig. 2B), ruling out these domains in mediating protein–protein interactions with KREL1. Previous yeast-2 hybrid data indicate the binding region on KREPA2 for KREL1 to be between residues 121–192 (Schnaufer et al. 2010). This region contains a predicted αH1 from conserved residues 146–166 (Supplemental Fig. S3). A pull-down test confirmed this region is the KREL1 binding site, as rKREPA2 with an internal deletion of this αH1 (Δ αH1) abolished the interaction (Fig. 2B).

The interaction between the αH3 of KREL1 CTD and αH1 of KREPA2 was further investigated through substitution mutation analyses where the hydrophobic, positively charged and negatively charged residues on both helices were substituted for alanine as separate group mutations. Group mutations of the positively charged lysine residues on KREL1 CTD αH3 led to a ~70% decrease in the binding efficiency to KREPA2 (Fig. 2C). Similarly, group mutations of negatively

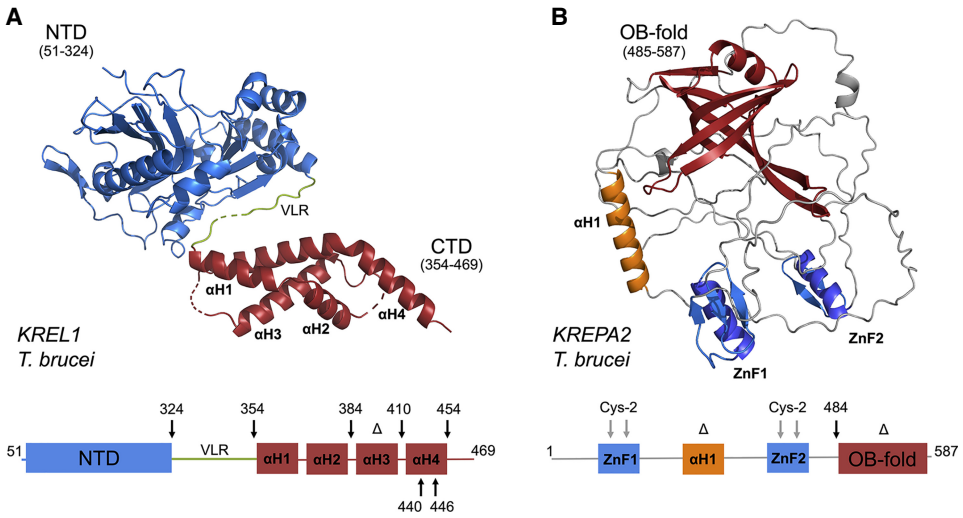

FIGURE 1. Full-length predicted structures of KREL1 and KREPA2. (*A*) Full-length Alphafold structure prediction of KREL1. The structure has two domains: NTD and CTD, which are connected by a variable loop region (VLR). The four-α helices of the CTD are labeled. A schematic of the mutations made on KREL1 is shown *below* the structure. The black arrows represent the site of the truncations and the Δ represents the internal helix deletion. (*B*) Full-length Alphafold structure prediction of KREPA2. The structure has an OB-fold domain, two ZnF domains and one α helix. A schematic of the mutations made on KREPA2 is shown *below* the structure. The black arrow at 484 represents the truncation made for the deletion of the OB-fold, the gray arrows represent the alanine substitutions of the cysteine residues of both ZnFs and Δ represents the internal deletion of the αH1.

charged glutamic and aspartic acid residues of KREPA2 αH1 led to a ~75% decrease in binding efficiency (Fig. 2C), revealing an electrostatic nature of KREL1–KREPA2 interaction. Mutations of the hydrophobic leucine residues of KREPA2 αH1 also resulted in a similar effect, although the latter was not seen in αH3 of KREL1 CTD. This suggests hydrophobic interactions with adjacent helices of KREL1 CTD for further stability, but not directly with αH3 (Fig. 2C).

In summary, we located the region of contact between KREL1 and KREPA2 to be between αH3 of KREL1 CTD and αH1 of KREPA2. The αH3 region of KREL1 is defined as a LAKD repeat motif that is completely absent in T4Rnl2, but highly conserved between trypanosomatid KRELs (Supplemental Fig. S1). Mutational analyses further confirm this to be driven through electrostatic interactions; the lysine residues of KREL1 αH3 form potential interactions with the glutamic and aspartic acid residues of KREPA2 αH1.

KREL1 CTD is required for ligase auto-adenylylation

To investigate the essentiality of KREL1's CTD in ligation, functional activities of KREL1 full-length (FL) and the truncated NTD (aa 51–324) were compared in vitro (Fig. 3A). The deletion of the CTD renders KREL1 inactive in the 3-step ligation assay as well as in the step 1 auto-adenylylation assay (Fig. 3B,C), as observed previously (Deng et al. 2004). The addition of KREPA2 enhances KREL1 FL auto-adenylylation activity, as shown earlier (Mehta et al. 2015), although it does not recover the lost activity of the KREL1 NTD construct, potentially due to the loss of its binding site (Fig. 3C). We also attempted salvaging KREL1 NTD's repressed auto-adenylylation activity by providing the purified CTD *in trans*, with and without KREPA2; however, no improvement was observed (Fig. 3C). It was not possible to experimentally test for KREL1 step 2 activity (RNA adenylylation) when the step 1 activity is abolished as a KREL1–AMP intermediate is required. However, step 3 (phospho-diester bond formation) activity can still be assessed with preadenylated RNA substrates. In the preadenylated ligation assay, KREL1's NTD (aa 51–324) is equally active as the KREL1 FL (Fig. 3D), suggesting that the CTD is not required for phosphor-diester formation. Point mutations of amino residues in the ATP binding pocket, including the conserved K87 of motif I, showed the essentiality of the residues from motifs I–V for steps 1 and 3 (data not shown) explaining that the ligase-ATP/AMP interaction occurs throughout the three-step ligation mechanism.

In summary, we show that the CTD of KREL1 is required for ligation activity, specifically for step 1. We also conclude that the NTD of KREL1 alone is required for the last step, by providing the AMP binding pocket interactions to catalyze the phosphor-diester bond formation.

KREL1 CTD harbors a diverged motif VI

As KREL1 NTD (aa 51–324) is inactive in adenylylation activity, we aimed to narrow the region of the CTD that is responsible for its essentiality in ATP hydrolysis. First, we tested the activity of the rKREL1 CTD truncations in our in vitro functional assays (Fig. 4A). While the truncations

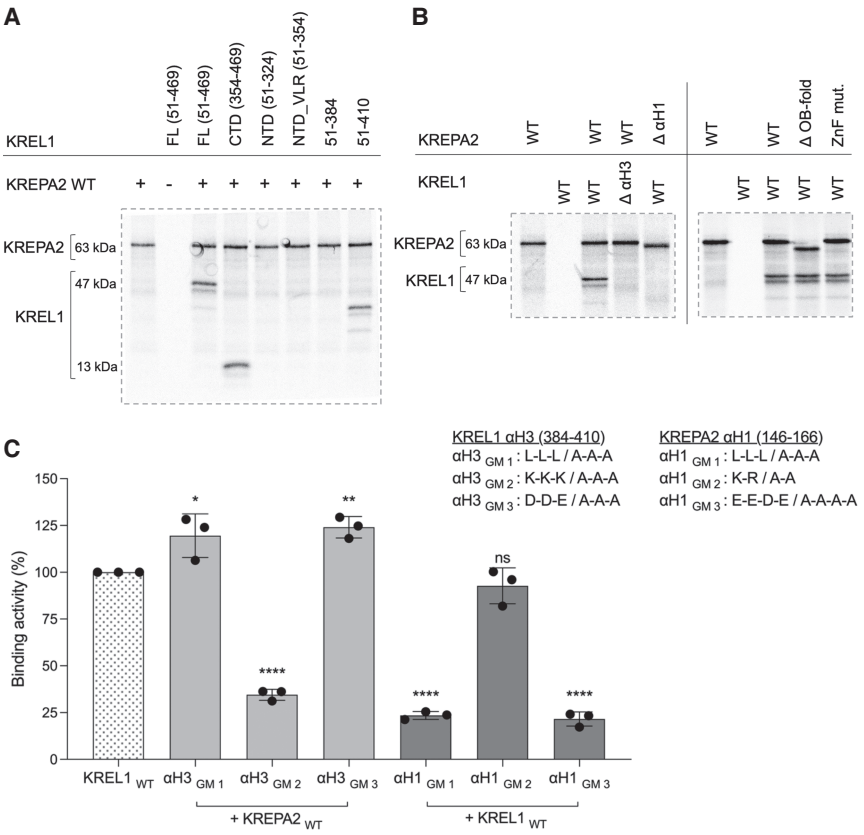

FIGURE 2. Pull-down assay of KREL1 with KREPA2. (*A*) Pull-down of KREPA2 wild-type (WT) with KREL1 full-length (FL), amino- and carboxy-terminal domains (NTD and CTD), and CTD truncations. (*B*) Pull-down of KREL1 WT and KREL1 ΔαH3 of the CTD with KREPA2 WT and domain mutants; deletion of αH1 (ΔαH1), deletion of OB-fold (ΔOB-fold) and ZnF mutant which substitutes four cysteine residues to alanine ($ZnF_{C/A}$). (*C*) Pull-down assay of group mutations (GM) of αH3 of KREL1 and αH1 of KREPA2. The light gray illustrates the KREL1 αH3 mutants with the addition of KREPA2 WT, and the dark gray illustrates the KREPA2 αH1 group mutants with KREL1 WT. GMs are detailed *next* to the graph, including alanine substitutions of positively charged residues, negatively charged residues, and hydrophobic residues on each helix. Error bars represent SD obtained from three replicate experiments. (****) $P < 0.0001$, (***) $P < 0.001$, (**) $P < 0.01$, (*) $P < 0.05$.

at residues 454 and 446 were functional in ligation and auto-adenylylation activities in vitro, truncation at residue 440 significantly impacted both processes (Fig. 4A,B). These truncations were also tested in the preadenylated ligation assay for which all truncated mutants were active, confirming the specific role of the CTD for step 1 (Supplemental Fig. S4). The region between residues 440–446 is located on αH4 of KREL1 CTD. A multiple sequence alignment of this region highlights four highly conserved residues, KWKE (441-444) between KREL1 and KREL2 of the kinetoplastid parasites (Supplemental Fig. 1). Single point mutations K441A, W442A, K443A, and K444A individually result in a reduction of KREL1–AMP formation by ~50%, ~75%, ~25% and ~30%, respectively (Fig. 4C). The 75% reduction in activity from W442A is salvageable with a synonymous mutation W442F, suggesting a primary role for W442 in pi-stacking interactions (Fig. 4C). Although point mutations partially affect KREL1 auto-adenylylation, group mutations of KWKE to AAAA and AWAA almost completely abolished activity (Fig. 4C–E). Moreover, we tested the KWKE group mutants in the presence of KREPA2 which was unable to rescue the loss of activity of these mutants (Fig. 4D,E).

These data narrow the region of KREL1 CTD important for ligase auto-adenylylation at the conserved KWKE motif. The essentiality of the KWKE residues in ATP hydrolysis is synonymous with the findings of mutational studies implemented in locating motif VI (RxDK) on DNA ligases (Sriskanda and Shuman 1998), suggesting the role of the CTD of KREL1 in providing a diverged motif VI-like region during the adenylylation step.

KREPA2 primes KREL1 for auto-adenylylation

While rKREL1 alone is sufficient for ligation activity in vitro, we examined the effect of KREPA2 on KREL1 activity to determine the functional impact of its interaction during the ligation mechanism. We performed several time-point experiments to measure the rate of KREL1 activity at each step of ligation and compared it with the addition of its interacting partner KREPA2 (Fig. 5). In the three-step ligation mechanism, KREL1 only ligates 40% of the input RNA in the first hour. Upon addition of KREPA2, efficiency increases by 30% (Fig. 5A). Using the KREPA2 ΔαH1 mutant, we showed that the deletion of the KREL1 binding site on KREPA2 results in baseline ligation efficiency, abolishing the enhancement effect (Fig. 5A). However, the deletion of the OB-fold domain or alanine substitutions of the cysteine residues in the ZnF domains on KREPA2, does not affect the increase in the rate of KREL1 ligation activity (Fig. 5B). A similarly designed experiment used radiolabeled ATP [α-^{32}P] to measure KREL1–AMP formation in the step 1 ligase auto-adenylylation assay. In the presence of KREPA2, there was an increase in KREL1 adenylylation activity and in the overall yield of this ligase intermediate; exhibited by the increased maximal binding capacity (B_{max}) of the curve (Fig. 5C), with no improvement in the apparent dissociation constant, K_d (data not shown). Step 2, ligase deadenylylation (RNA adenylylation) activity, was assessed

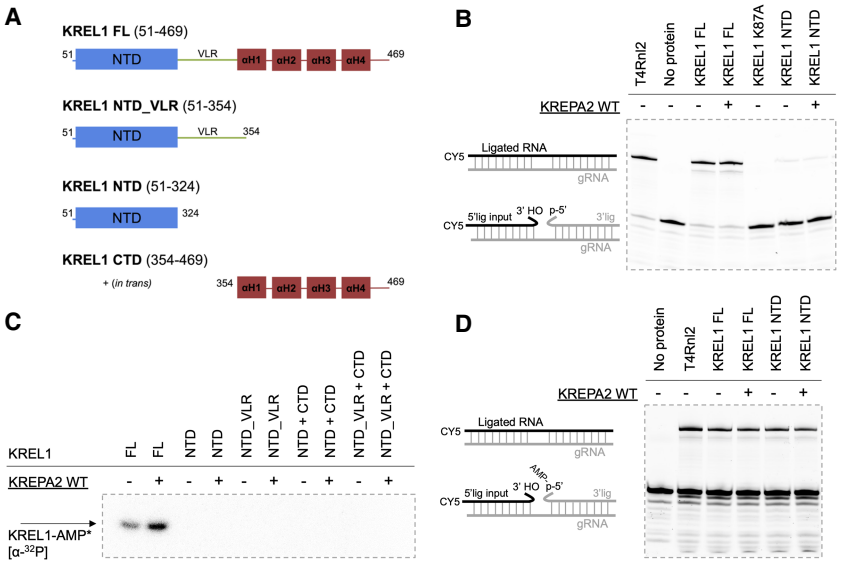

FIGURE 3. In vitro functional assays of KREL1 full-length and domain truncated mutants with and without KREPA2. (*A*) Structural representation of the KREL1 constructs used including full-length (FL), NTD, NTD_VLR and the CTD provided in *trans*. (*B*) Three-step ligation assay of KREL1 FL vs. NTD, with and without KREPA2 WT. T4Rnl2 was used as a positive control, and KREL1 K87A was used as a negative control. Identities of RNA species are depicted to the *left* of the gels. The RNA being visualized contains a CY5 label. (*C*) Ligase auto-adenylylation assay, representative of step 1 of ligation, of KREL1 FL and domain, truncated mutants with and without KREPA2. A "+" symbol represents reactions with domains provided in *trans*. The KREL1–AMP product is radiolabeled with α-^{32}P represented by an asterisk. (*D*) Preadenylated ligation assay, representative of step 3 of ligation, of KREL1 FL vs. NTD with and without KREPA2. T4Rnl2 was used as a positive control. The RNA being visualized contains a CY5 label.

by observing the decrease in the radiolabeled KREL1–AMP in the presence of ligatable RNA substrates. Although no significant change in the rate of ligase deadenylylation was observed with the addition of KREPA2, represented by the curve slope, an increased percentage of KREL1–AMP intermediate remained in the presence of KREPA2 (Fig. 5D). In the isolated step 3 ligase activity assay (preadenylated ligation), the ligation rate was slower in the presence of KREPA2 in vitro (Fig. 5E); suggesting either the need for KREPA2 to dissociate from KREL1 in the final step (3) of ligation or this is a rate-limiting step specific to the KRELs assuming KREPA2 dissociation does not occur.

In summary, the interaction between KREL1 and KREPA2 increases the efficiency of KREL1 ligation, specifically for auto-adenylylation. We also show that the OB-fold and ZnF domains of KREPA2 do not directly impact the RNA ligation mechanism of KREL1 in vitro.

DISCUSSION

The major findings of this study can be summarized as follows. First, KREL1 possesses an α-helix (αH3) on its CTD, forming a physical interaction with αH1 of its binding partner KREPA2. Second, the CTD of KREL1 is essential in the auto-adenylylation reaction by providing a functional motif VI, KWKE, which interacts with ATP during hydrolysis. Third, KREPA2 increases the efficiency of KREL1 adenylylation activity in vitro mediated by its interaction with no apparent role of its OB-fold or ZnFs in ligation.

Our analysis of KREL1 and KREPA2 initiates from sequence alignments and predicted structures from Alphafold Colab database (Fig. 1; Jumper et al. 2021; Varadi et al. 2022). The full-length KREL1 protein, without its mitochondrial import signal, harbors a ~34 kDa ATP-hydrolysis amino-terminal domain (51–324). The ATP-binding pocket is composed of Motifs (I, III, IIIa, IV, V) that are conserved in the family of nucleotidyl transferases (Doherty and Suh 2000). The multiple sequence alignment of the KRELs from the three major kinetoplastid parasites and their closest known ortholog, bacteriophage T4 RNA ligase 2 (T4Rnl2), highlight these conserved motifs (Supplemental Fig. S1; Ho and Shuman 2002). As the predicted KREL1 structure shows, the NTD is linked to a ~13 kDa carboxy-terminal domain (CTD) through a variable loop region (VLR) that likely provides flexibility in engaging/disengaging the interactions between the two domains supported by our inability to obtain KREL1 activity with the domains provided *in trans* (Fig. 3C). The CTD is comprised of four α-helices: αH1 (aa 357–367), αH2 (aa 370–380), αH3 (aa 392–410), and αH4 (aa 419–456). Through our mutational analysis of KREL1 in protein–protein interaction and in vitro ligation activity, we identified two critical regions of interest on the CTD: αH3 (aa 392–410) as the KREPA2 binding site and KWKE motif (aa 441–444) as the diverged motif VI (Supplemental Fig. S1).

Previous work investigated the CTD of KREL1 through LAMA analysis and MEME motif database search and found aa 381–383 region similar to a motif found in microtubule-associated tau proteins (IPB0011084D) (Worthey et al. 2003). Protein Tau binds microtubules through short sequence motif repeats, with a KxGS signature (Avila et al. 2019). This region of KREL1, KIG (aa 381–383), noted as microtubule-associated tau was, however, ruled out to be involved in the KREPA2 interaction with our pull-down assay as KREL1 384 truncation (aa 51–384) was unable to bind to KREPA2 (Fig. 2). Interestingly, the stretch of residues before the KXGS motif of Tau shares similarities to the αH3 of KRELs (Avila et al. 2019). Within this region of Tau, mutational analysis of the tau protein revealed the importance of the lysine residues for this interaction (Goode

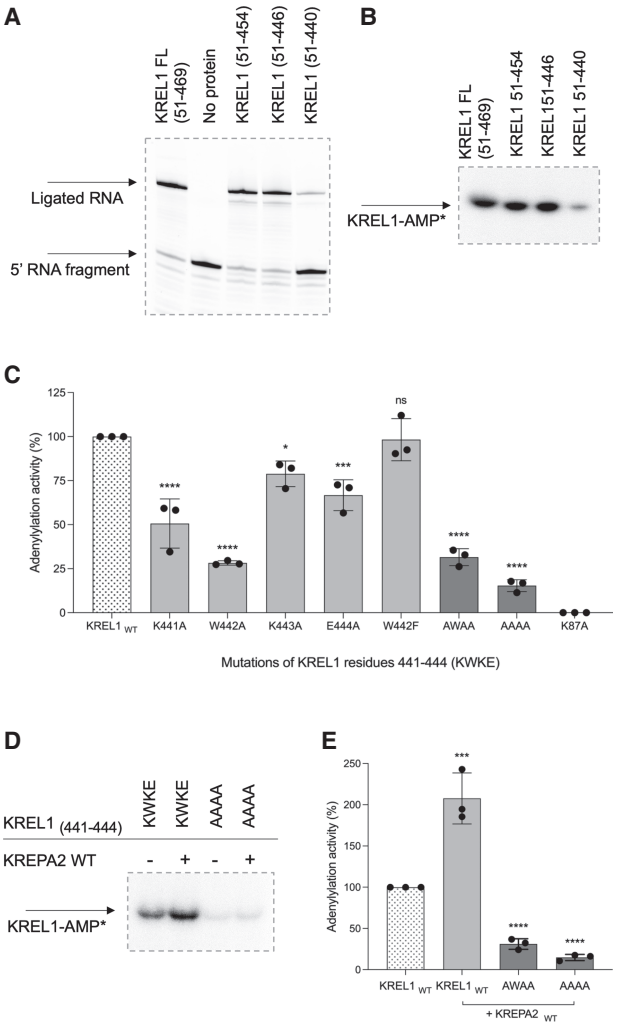

FIGURE 4. Locating motif VI on KREL1 carboxy-terminal domain. (*A*) Three-step ligation assay with KREL1 FL and CTD truncations. (*B*) Adenylylation assay with KREL1 FL and CTD truncations. (*C*) Adenylylation assay of KREL1 WT and group mutants (alanine substitutions for residues 441–444, KWKE) with and without the addition of KREPA2. (*D*) Adenylylation of point mutants and group mutants of KREL1, compared to adenylylation activity of KREL1 WT. Group mutants (GM) include KWKE substituted for AWAA and AAAA. (*E*) Adenylylation assay of KREL1 WT and group mutants with the addition of KREPA2 WT. Error bars on each graph represent SD obtained from three replicate experiments. (****) $P < 0.0001$, (***) $P < 0.001$, (**) $P < 0.01$, (*) $P < 0.05$.

et al. 1997, 2000). Consistent with this conclusion, our work supports the essentiality of the positively charged lysine residues of αH3 of KREL1 CTD in the interaction with KREPA2.

The essentiality of the CTD in KREL1 auto-adenylylation suggests a region of critical residues that are required for the proper hydrolysis of ATP. The region, KWKE (aa 441–444) is synonymous with the RxDK motif previously described in DNA ligases and mRNA capping enzymes that interact with ATP in the binding pocket prior to adenylylation (Subramanya et al. 1996; Håkansson et al. 1997; Sriskanda and Shuman 1998). Specifically, the arginine and lysine residues of RxDK motif VI in DNA ligases interact with the β- and γ-phosphates for the proper orientation of the ATP molecule for the covalent bond to form between the K of motif I and AMP. We suggest a similar interaction between the lysine residues of KWKE and the β- and γ-phosphates to enable the hydrolysis of ATP and the release of pyrophosphate. Highlighted in a multiple sequence alignment, these residues are highly conserved in the KRELs while loosely conserved in T4Rnl2 (Supplemental Fig. S1). Although the NTD of T4Rnl2 is functionally independent of its CTD in adenylylation (Ho et al. 2004), the author notes an increase in the ideal pH condition to be more alkaline, likely aiding in the de-protonation of the lysine residue of motif I for covalent bond formation. We have shown that pH 8.0 is the optimal condition of KREL1 adenylylation (Supplemental Fig. S5), although the KREL1 NTD alone was inactive in all pH conditions. We believe the motif VI of KRELs is provided to the binding pocket to aid in ATP hydrolysis and potentially maintain the pH of the microenvironment required for covalent bond formation.

KREL1's ~63 kDa interacting partner, KREPA2, contains two recognizable zinc-finger domains (ZnF1 and ZnF2) flanking a 20-residue α-helix (αH1) and a carboxy-terminal OB-fold domain (Fig. 1). The OB-fold domains conserved in all the six RECC KREPA proteins are essential for the integrity of the complex as they are potentially involved in protein–protein interactions that make up the scaffolding of the RECC (Schnaufer et al. 2010). Of the six KREPA proteins, KREPA1–3 each share two classical C2H2 zinc fingers (Cys2–His2) of 24 aa comprised of a left-handed ββα structure, involved in nucleic acid binding and protein–protein binding (Supplemental Fig. S3B; Matthews and Sunde 2002; Brayer and Segal 2008; Fedotova et al. 2017). For example, KREPA3 ZnFs seem to play a role in RNA editing efficiency, likely by mediating RECC–RNA interactions (Guo et al. 2010), while the KREPA2 ZnF1 was shown to be involved in complex assembly, potentially by integrating the deletion subcomplex into the RECC core similar to the OB-fold. Our mutational analysis of KREPA2 showed no significant change with the deletion of the OB-fold or mutations of the ZnFs, in both KREL1 interaction and KREL1 ligation and auto-adenylylation activities (Figs. 2, 5). While these domains may not play a role in KREL1 RNA ligation directly, the question remains if these domains have a role in RNA interaction, possibly downstream from the editing site in conjunction with the other KREPA proteins of the complex.

Unlike KREPA3, KREPA1, and KREPA2 harbor a highly conserved α-helix between the ZnF domains, containing several exposed charged residues (Supplemental Fig. S3C). This region was narrowed to be the binding site of KREL1 αH3. The conservation of αH1 in both KREPA2 and KREPA1 proteins may indicate an analogous

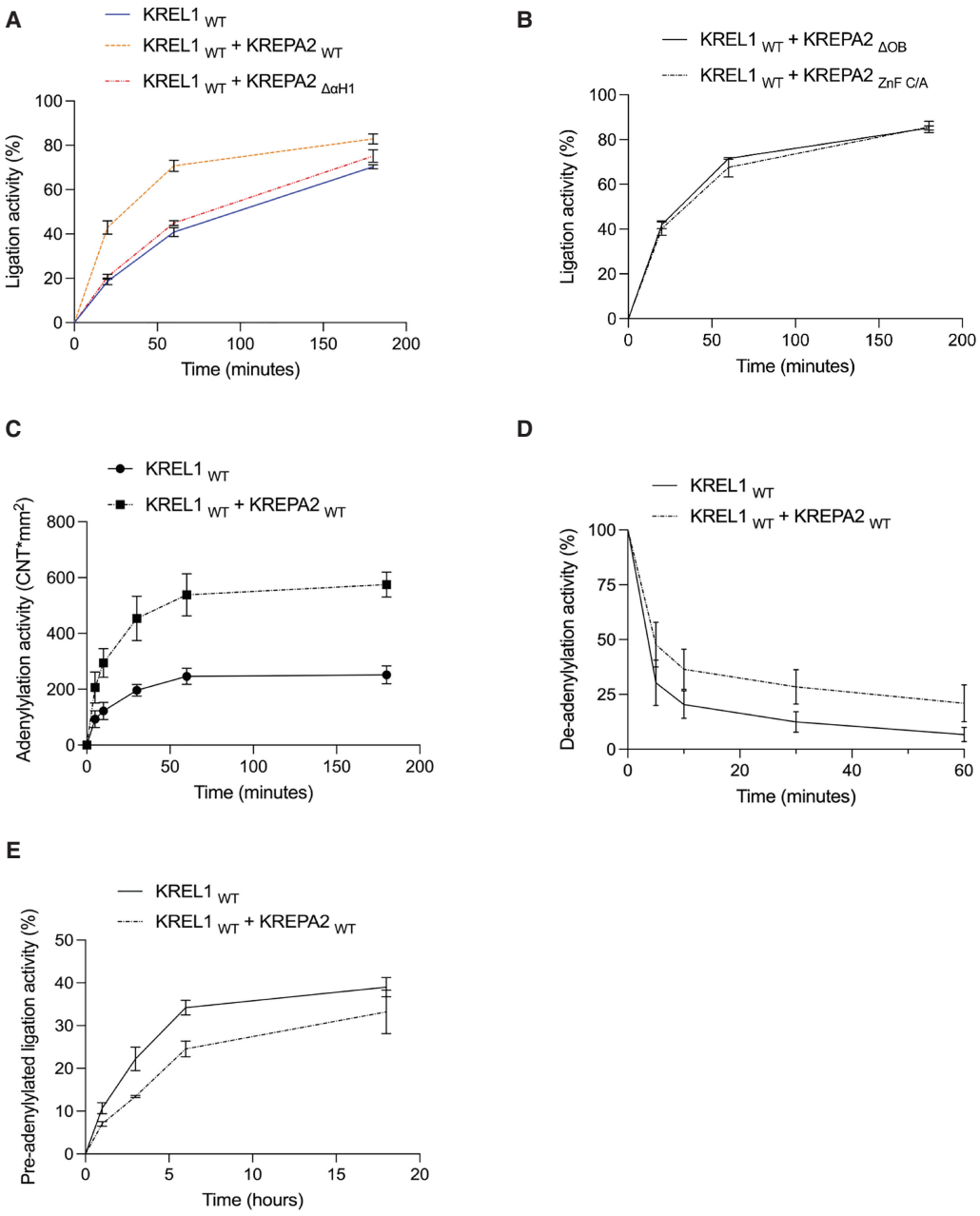

FIGURE 5. In vitro functional assays of KREL1 with and without KREPA2 over time. (*A*) Three-step ligation activity over time of KREL1 WT with and without the addition of KREPA2 WT and KREPA2 ΔαH1 mutant. (*B*) Two other conditions, KREL1 WT with KREPA2 ΔOB mutant and KREPA2 ZnF mutant (alanine substitutions of cysteine residues), were extracted from the graph of panel *A* for easier visualization. (*C*) KREL1 adenylylation activity over time with and without the addition of KREPA2 WT. (*D*) KREL1 deadenylylation activity over time with and without the addition of KREPA2 WT. (*E*) KREL1 preadenylated ligation activity over time with and without the addition of KREPA2 WT. Error bars on each graph represent SD obtained from three replicate experiments.

interaction between the paralogs KREL2–KREPA1. The high degree of similarity between these binding sites may be a possible explanation for the ability of KREL1 to rescue RNA editing and cell viability in KREL2 knockdown mutants (Schnaufer et al. 2001) through binding to KREPA1 to take part in the U-insertion subcomplex. However, no data have been shown to support this to date.

The effect of KREPA2 on KREL1 ligation activity is an increase in the efficiency of KREL1 auto-adenylylation mediated by the αH3–αH1 interaction between KREL1 CTD and KREPA2. In our in vitro functional analysis of the adenylylation step, the overall yield of KREL1–AMP formation increases in the presence of KREPA2. KREPA2's role appears to be specific to step 1 as there was no significant

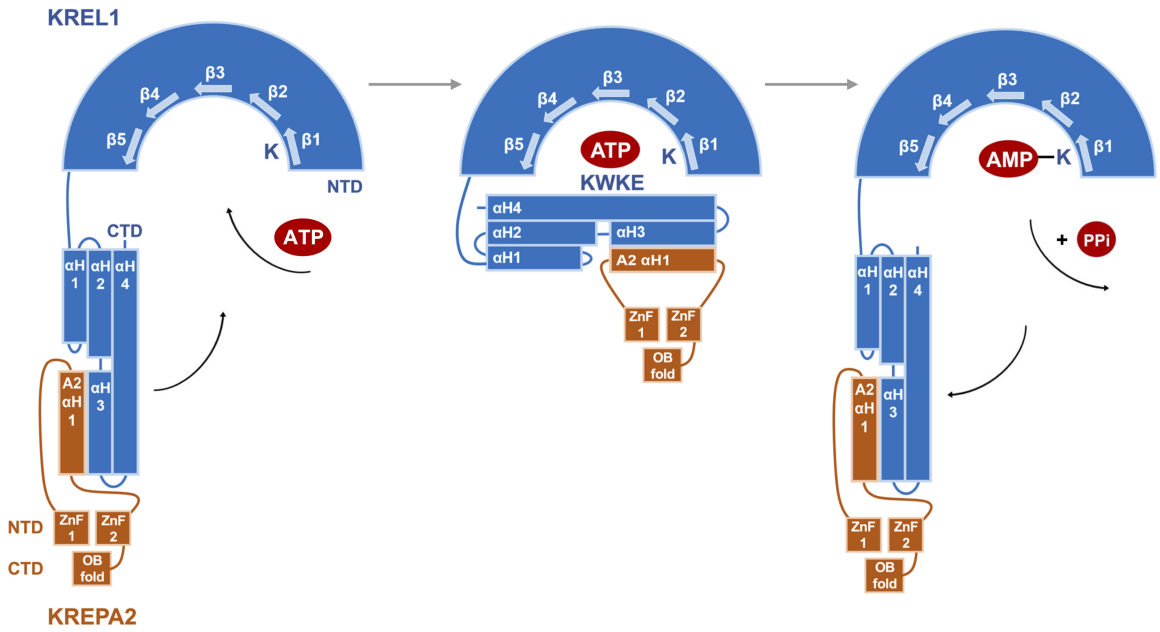

FIGURE 6. Model for ligase auto-adenylylation. Mechanism of KREL1 adenylylation, representative of step 1 of ligation, in the presence of KREPA2. (*Left*) KREL1 (in blue) is shown with its amino terminus with five β sheets that make up the ATP binding pocket. The VLR connects the NTD to a four-helix domain at the carboxyl terminus. KREL1 begins in the open conformation with KREPA2 (in orange) αH1 bound to KREL1 αH3 CTD. (*Center*) In the presence of ATP in the binding pocket, the CTD is shown to fold onto its NTD in the closed conformation. The ligase catalyzes a covalent linkage between a lysine of motif I (depicted as the "K" protruding from β sheet 1) with the α-phosphate of ATP. Motif VI, KWKE, on αH4 is involved in adenylylation to form the KREL1–AMP intermediate. (*Right*) The ligase opens to release pyrophosphate and proceed in the ligation reaction. KREPA2's interaction mediates the conformational changes.

improvement in KREL1 activity in steps 2 and 3 in our in vitro functional assays. KREL1 NTD is active independent of its CTD in step 3, suggesting that KREPA2 interaction is not required and may be unfavorable. As KREPA2 interacts with the CTD of KREL1, the domain that is essential for ATP-hydrolysis, and further increases the efficiency of KREL1 adenylylation activity, we suggest that KREPA2's role mediates the conformational change necessary for this step and regulates the accessibility of these domains.

Based on the results from this work, a model of the ligase-adenylate formation is compatible with the open-closed conformational changes observed with structurally resolved GTPase capping enzymes and DNA ligases (Fig. 6; Håkansson et al. 1997; Unciuleac et al. 2019). The uniqueness of KREL1 is that the conformational change required for auto-adenylylation is improved with KREPA2 interaction. Initially, the KREL1 enzyme is required in an open conformation to accept ATP for adenylylation. Critical residues of motif I–VI form interactions with ATP. For a covalent bond to form between the K87 of motif I and AMP, residues in motif VI (KWKE) are required to interact and orient the β- and γ-phosphates of the ATP molecule. Such interaction is provided in a closed conformation, mediated by KREPA2's interaction. This is consistent with the unprocessed ATP in the crystalized NTD of KREL1 (PDB code 1XDN) that was missing the motif VI from the CTD for proper orientation and hydrolysis with K87 of motif I. An open conformation at the final stage of ligation, phospho-diester bond formation, is suggested to interact with the dsRNA whereby motif VI or KREPA2 are not required for activity. KREL1 CTD is always to be imagined with KREPA2 αH1 for RECC integration and for optimal movement in assisting KREL1's conformational change for ligase auto-adenylylation via involvement of a motif VI-like region (KWKE), critical for adenylylation.

Concluding comments

Using biochemical and structural data, we report two distinct structural motifs of *T. brucei* KREL1 CTD; motif VI explicitly recognizes ATP to form the ligase-adenylate and the αH3 region that interacts with the KREPA2 binding partner. The interaction of KREPA2 through its αH1 modulates ligation in the first step, likely by promoting the closure of the KREL1 motif VI onto the ATP binding pocket.

Whereas other characterized ligases such as T7 DNA ligase have a catalytic domain and an OB-fold domain along with motif VI, KREL1 contains only the catalytic domain with a motif VI in its CTD, with the OB-fold domain provided in *trans* by KREPA2 for ligation. Our results indicate a diverged version of this motif VI, specific to kinetoplastid RNA editing ligases, located on the CTD similar to other ligases, albeit without an adjacent OB-fold domain.

In the KREL1 ligation mechanism, our data indicate no apparent role for the OB-fold.

MATERIALS AND METHODS

Sequence alignment and structure predictions

Amino acid sequences of KREL1 and KREPA2 from *T. brucei* and related species were extracted from the TriTryp database (https://tritrypdb.org/tritrypdb/app) and aligned to related proteins using Clustal Omega (Sievers et al. 2011). We excluded the 50 amino acid mitochondrial import signal of kinetoplastid RNA ligases. Structural predictions of KREL1 and KREPA2 were achieved using the AlphaFold Colab database developed by DeepMind and EMBL's European Bioinformatics Institute (Jumper et al. 2021; Varadi et al. 2022) and used in the analysis of the structural domains (Fig. 1; Supplemental Fig. S3).

Cloning of full-length KREL1 and KREPA2

KREL1 FL (51–469) of *T. brucei* was cloned in pET30b as previously described (Mehta et al. 2015) to express rKREL1 with an amino-terminal 6× his-tag. *T. brucei* KREPA2 (1–587) was excised from a pSG1-KREPA2 construct and cloned into a pLEXSY_invitro-2 plasmid (www.jenabioscience.com) then outsourced for -TAP-tag fusion plasmid by GenScript Corporation. The expressed rKREPA2 contains a carboxy-terminal affinity purification tag, with a calmodulin tag—TEV protease site—6× his-tag. The advantages of using this plasmid were efficient affinity chromatography purification and western blot analysis for quantification.

Cloning of KREL1 and KREPA2 truncations and mutants

A summary of the truncations, point mutations, and group mutations performed on KREL1 and KREPA2 are listed in Supplemental Table S1. For KREL1, DNA fragments were generated by PCR between restriction enzymes KpnI and XhoI using the wild-type KREL1 construct. For KREPA2, DNA fragments were generated by PCR between restriction enzymes NcoI and XbaI using the wild-type KREPA2 construct. Plasmid preparation of KREL1 and KREPA2 mutants was prepared by GenScript Corporation. Mutations on KREL1 are marked in the multiple sequence alignment (Supplemental Fig. S1), and mutations on KREPA2 are marked in the multiple sequence alignment (Supplemental Fig. S3).

Expression and purification of recombinant KREL1 and KREPA2

The rKREL1 and rKREPA2 wild-type and mutant proteins were expressed in vitro with a reticulocyte lysate-based cell-free coupled transcription and translation system (TnT) (Cat. # L1170, Promega). Proteins were expressed with [35S] methionine (NEG709A500UC, PerkinElmer), and used directly for the pull-down assay. An aliquot of the expressed protein was resolved in an SDS-PAGE gel (Supplemental Fig. S2). For in vitro functional assays, proteins were expressed with TnT and purified.

For rKREL1 purification, TnT reactions post incubation were added to magnetic nickel beads (Dynabeads; 00972814, Invitrogen) in binding buffer (25 mM NaPO4 [pH 8.0], 200 mM NaCl and 0.01% Tween 20) and rotated at 4°C for 1 h. Using a magnetic rack, the supernatant was removed, and the beads were subsequently washed three times with binding buffer. The beads were then added to an elution buffer (50 mM NaPO4 [pH 8.0], 300 mM NaCl, 0.01% Tween 20, and 300 mM Imidazole) and rotated at 4°C for 45 min.

For rKREPA2 purification, TnT reactions post incubation were added to calmodulin resin beads (CRB) in binding buffer (10 mM Tris-HCl [pH 8.0], 150 mM NaCl, 0.1%NP40, 2 mM β-ME, 1 mM Mg Acetate, 1 mM imidazole, and 2 mM $CaCl_2$) and rotated at 4°C for 2 h. The beads were briefly spun down to remove the supernatant and washed with a binding buffer three times. CRB were then suspended in elution buffer (10 mM Tris-HCl [pH 8.0], 150 mM NaCl, 0.1%NP40, 10 mM β-ME, 1 mM Mg-acetate, 1 mM imidazole, and 2 mM EGTA) and rotated at 4°C for 1 h.

The eluates containing either rKREL1 or rKREPA2 were buffer exchanged in 1× HHE (25 mM HEPES, 10 mM $Mg(OAc)_2$, 1 mM EDTA, 50 mM KCl) and further concentrated using 10K Amicon Ultra centrifugal filters (R1CB94236, Sigma Aldrich). Recombinant proteins were examined by western blotting using an anti-His-tag antibody (631212, Clontech) and visualized with ChemiDoc (Bio-Rad) (Supplemental Fig. S2). A His-tagged protein ladder was loaded in increasing amounts of 20, 40, 80, and 120 ng to calculate a standard curve for the quantification of recombinant proteins.

KREPA2 pull-down assay

Recombinant proteins were radiolabeled with [^{35}S] methionine using the TnT expression system. An aliquot of the reactions was loaded on an SDS-PAGE gel to visualize expression (Supplemental Fig. S2). Equal volumes of rKREL1 TnT reaction and rKREPA2 TnT reaction were mixed on ice for 15 min. KREPA2, with its calmodulin tag, would bind to the CRB and pull-down KREL1. The mixed reactions were suspended in binding buffer (10 mM Tris-HCl [pH 8.0], 150 mM NaCl, 0.1%NP40, 2 mM β-ME, 1 mM Mg Acetate, 1 mM imidazole, and 2 mM $CaCl_2$) and rotated at 4°C for 2 h with CRB. Supernatants were removed, and CRB was subsequently washed three times with a binding buffer. The supernatants were removed using ZEBA micro spin 10 kD columns (Cat No: P189879), and the CRB was subsequently washed three more times, each time spun through the column. CRB were then suspended in elution buffer (10 mM Tris-HCl [pH 8.0], 150 mM NaCl, 0.1% NP40, 10 mM β -ME, 1 mM Mg Acetate, 1 mM imidazole, and 10 mM EGTA). Eluted proteins were denatured with SDS loading dye, migrated in a 10% SDS-PAGE gel, exposed to an X-ray film, and visualized using a PhosphoImager (Bio-Rad). Analysis was conducted using Quantity-one software (Bio-Rad).

Three-step ligation assay

KREL1 ligation activity was studied in vitro using annealed dsRNA. 2 μM of 5′ labeled CY5 5′RNA fragment (5′-GGA AAGUUGUGACUGA-3′) and 2 μM of 3′RNA fragment (5′-pUG AGUCCGUGAGGACGAAACAAUAGAUCAAAUGUp-3′) were

annealed to a 4 µM guide RNA (5′-GUUUUGUUCUUAUGGA CUCAUCAGUCAUAAUUUUCCUU-3′) in 2x HHE buffer.

The RNA fragments were placed in a water bath at 70°C and cooled to RT. The dsRNA was then added to a ligation reaction (2× HHE [pH 8.0], $CaCl_2$, Tx-100, ATP, RNAase inhibitor) with 1 pmol of rKREL1 ± rKREPA2 proteins. The reactions were incubated overnight and at various time points, at 28°C in the dark, shaking at 50 rpm. The reactions were quenched by adding 20 µM guide RNA competitor (DNA) (5′-AAAAAAAAAAGGAAAAT TATGACTGAGTGAGTCCATAAGAACAAAAC-3′) and equal volume of 10 M Urea in TBE and heated at 95°C for 90 sec. The RNA was resolved on a 20% acrylamide gel (37:1) and visualized at ~650 nm for CY5 using a ChemiDoc (Bio-Rad) machine. Analysis was conducted using ImageLab software (Bio-Rad).

Step 1, ligase adenylylation assay

KREL1 auto-adenylylation activity was studied in vitro with [α-^{32}P] ATP. Reactions were set up with 0.2 pmol of KREL1 ± KREPA2 along with 1 µCi [α-^{32}P] ATP in a solution containing 25 mM Tris-HCl [pH 8.0], 10 mM $Mg(OAc)_2$, 0.5 mM DTT, 1% BSA, and 10% DMSO at RT. Reactions were optimized at pH 8.0 (Supplemental Fig. S5). The reactions were incubated for 10 min and at various time points, at RT. Reactions were quenched with SDS-loading dye, migrated on a 10% SDS-PAGE gel, exposed to an X-ray film, and visualized using a PhosphorImager (Bio-Rad). Analysis was conducted using Quantity One software (Bio-Rad).

Step 2, RNA adenylylation assay

KREL1 deadenylylation activity was studied in vitro in the presence of nicked dsRNA as described in the ligation assay. Adenylylated KREL1 with [α-^{32}P] ATP, as described in the adenylylation assay, was added to dsRNA mixtures detailed in the three-step ligation assay. The rate of reaction was examined in the presence of KREPA2 and compared to the rate of KREL1 deadenylylation. Reactions were quenched at different time points with the denaturing SDS-loading dye and visualized with methods of all radioactive assays.

Step 3, preadenylated ligation assay

KREL1 phosphodiester bond formation activity was studied in vitro using a preadenylated dsRNA. For this assay, the 3′ RNA fragment was first adenylylated using a 5′ DNA adenylation kit (NEB, catalog # E2610S). It contains a *Methanobacterium thermoautotrophicum* ligase that adenylates a nucleic acid strand at the 5′ end. The RNA was purified through ethanol precipitation and migrated through an acrylamide gel for verification (Supplemental Fig. S6). Next, 2 µM of 5′ labeled CY5 RNA fragment and 2 µM of preadenylated 3′ RNA fragment were annealed to 4 µM guide RNA in 2× HHE. The RNA fragments were placed in a water bath at 70°C and cooled to RT. The RNA mix was then added to a reaction (2× HHE [pH 8.0], $CaCl_2$, Tx-100, and RNase inhibitor) with 1 pmol of KREL1 ± KREPA2 protein. It should be noted that this assay lacked the addition of ATP.

The reactions were incubated overnight and at various time points; at 28°C in the dark while shaking at 50 rpm. The reactions were quenched by adding 20 µM guide RNA competitor (DNA) and an equal volume of 10 M Urea in TBE and heated at 95°C for 90 sec. The RNA was resolved on a 20% acrylamide gel (37:1) and visualized at ~650 nm for CY5 using a ChemiDoc (Bio-Rad) machine. Analysis was conducted using ImageLab software (Bio-Rad).

SUPPLEMENTAL MATERIAL

Supplemental material is available for this article.

ACKNOWLEDGMENTS

We thank Akshaya Srikanth for assistance with the recombinant protein expression and purification optimization, Mojtaba Rostamighadi for assistance with fluorescence RNA assays, and Lin Hua Zhang for help in plasmid design. The research in the Salavati laboratory is supported by the Natural Sciences and Engineering Research Council of Canada (NSERC), grant number RGPIN 328186.

Received August 25, 2022; accepted October 31, 2022.

REFERENCES

Alalaiwe A, Wang PW, Lu PL, Chen YP, Fang JY, Yang SC. 2018. Synergistic anti-MRSA activity of cationic nanostructured lipid carriers in combination with oxacillin for cutaneous application. *Front Microbiol* **9:** 1493. doi:10.3389/fmicb.2018.01493

Aphasizhev R, Aphasizheva I. 2014. Mitochondrial RNA editing in trypanosomes: small RNAs in control. *Biochimie* **100:** 125–131. doi:10.1016/j.biochi.2014.01.003

Avila J, Jadhav S, Di Primio C, Devred F, Landrieu I, Barbier P, Zejneli O, Martinho M, Lasorsa A, Belle V, et al. 2019. Role of tau as a microtubule-associated protein: structural and functional aspects. *Front Aging Neurosci* **100:** 125–131. doi:10.3389/fnagi.2019.00204

Brayer KJ, Segal DJ. 2008. Keep your fingers off my DNA: protein–protein interactions mediated by C2H2 zinc finger domains. *Cell Biochem Biophys* **50:** 111–131. doi:10.1007/s12013-008-9008-5

Deng J, Schnaufer A, Salavati R, Stuart KD, Hol WGJ. 2004. High resolution crystal structure of a key editosome enzyme from *Trypanosoma brucei*: RNA editing ligase 1. *J Mol Biol* **343:** 601–613. doi:10.1016/j.jmb.2004.08.041

Doherty AJ, Suh SW. 2000. Structural and mechanistic conservation in DNA ligases. *Nucleic Acids Res* **28:** 4051–4058. doi:10.1093/nar/28.21.4051

Ellenberger T, Tomkinson AE. 2008. Eukaryotic DNA ligases: structural and functional insights. *Annu Rev Biochem* **77:** 313–338. doi:10.1146/annurev.biochem.77.061306.123941

Fedotova AA, Bonchuk AN, Mogila VA, Georgiev PG. 2017. C2H2 zinc finger proteins: the largest but poorly explored family of higher eukaryotic transcription factors. *Acta Naturae* **9:** 47–58. doi:10.32607/20758251-2017-9-2-47-58

Flynn RL, Zou L. 2010. Oligonucleotide/oligosaccharide-binding fold proteins: a growing family of genome guardians. *Crit Rev Biochem Mol Biol* **45:** 266–275. doi:10.3109/10409238.2010.488216

Goode BL, Denis PE, Panda D, Radeke MJ, Miller HP, Wilson L, Feinstein SC. 1997. Functional interactions between the proline-rich and repeat regions of tau enhance microtubule binding and assembly. *Mol Biol Cell* **8:** 353. doi:10.1091/mbc.8.2.353

Goode BL, Chau M, Denis PE, Feinstein SC. 2000. Structural and functional differences between 3-repeat and 4-repeat tau isoforms. Implications for normal tau function and the onset of neurodegenerative disease. *J Biol Chem* **275:** 38182–38189. doi:10.1074/jbc.M007489200

Guo X, Ernst NL, Stuart KD. 2008. The KREPA3 zinc finger motifs and OB-fold domain are essential for RNA editing and survival of *Trypanosoma brucei*. *Mol Cell Biol* **28:** 6939–6953. doi:10.1128/MCB.01115-08

Guo X, Ernst NL, Carnes J, Stuart KD. 2010. The zinc-fingers of KREPA3 are essential for the complete editing of mitochondrial mRNAs in *Trypanosoma brucei*. *PLoS ONE* **5:** e8913. doi:10.1371/journal.pone.0008913

Håkansson K, Doherty AJ, Shuman S, Wigley DB. 1997. X-ray crystallography reveals a large conformational change during guanyl transfer by mRNA capping enzymes. *Cell* **89:** 545–553. doi:10.1016/S0092-8674(00)80236-6

Ho CK, Shuman S. 2002. Bacteriophage T4 RNA ligase 2 (gp24.1) exemplifies a family of RNA ligases found in all phylogenetic domains. *Proc Natl Acad Sci* **99:** 12709–12714. doi:10.1073/pnas.192184699

Ho CK, Wang LK, Lima CD, Shuman S. 2004. Structure and mechanism of RNA ligase. *Structure* **12:** 327–339. doi:10.1016/j.str.2004.01.011

Huang CE, O'Hearn SF, Sollner-Webb B. 2002. Assembly and function of the RNA editing complex in *Trypanosoma brucei* requires band III protein. *Mol Cell Biol* **22:** 3194–3203. doi:10.1128/MCB.22.9.3194-3203.2002

Jensen RE, Englund PT. 2012. Network news: the replication of kinetoplast DNA. *Annu Rev Microbiol* **66:** 473–491. doi:10.1146/annurev-micro-092611-150057

Jumper J, Evans R, Pritzel A, Green T, Figurnov M, Ronneberger O, Tunyasuvunakool K, Bates R, Žídek A, Potapenko A, et al. 2021. Highly accurate protein structure prediction with AlphaFold. *Nature* **596:** 583–589. doi:10.1038/s41586-021-03819-2

Kable ML, Seiwert SD, Heidmann S, Stuart K. 1996. RNA editing: A mechanism for gRNA-specified uridylate insertion into precursor mRNA. *Science* **273:** 1189–1195. doi:10.1126/science.273.5279.1189

Martins A, Shuman S. 2004. An RNA ligase from *Deinococcus radiodurans*. *J Biol Chem* **279:** 50654–50661. doi:10.1074/jbc.M407657200

Matthews JM, Sunde M. 2002. Zinc fingers: folds for many occasions. *IUBMB Life* **54:** 351–355. doi:10.1080/15216540216035

Mehta V, Sen R, Moshiri H, Salavati R. 2015. Mutational analysis of *Trypanosoma brucei* RNA editing ligase reveals regions critical for interaction with KREPA2. *PLoS ONE* **10:** e0120844. doi:10.1371/journal.pone.0120844

Nandakumar J, Shuman S, Lima CD. 2006. RNA ligase structures reveal the basis for RNA specificity and conformational changes that drive ligation forward. *Cell* **127:** 71–84. doi:10.1016/j.cell.2006.08.038

Ramrath DJF, Niemann M, Leibundgut M, Bieri P, Prange C, Horn EK, Leitner A, Boehringer D, Schneider A, Ban N. 2018. Evolutionary shift toward protein-based architecture in trypanosomal mitochondrial ribosomes. *Science* **362:** eaau7735. doi:10.1126/science.aau7735

Samai P, Shuman S. 2012. Kinetic analysis of DNA strand joining by *Chlorella* virus DNA ligase and the role of nucleotidyltransferase motif VI in ligase adenylylation. *J Biol Chem* **287:** 28609–28618. doi:10.1074/jbc.M112.380428

Schnaufer A, Panigrahi AK, Panicucci B, Igo RP, Salavati R, Stuart K. 2001. An RNA ligase essential for RNA editing and survival of the bloodstream form of *Trypanosoma brucei*. *Science* **291:** 2159–2162. doi:10.1126/science.1058955

Schnaufer A, Ernst NL, Palazzo SS, O'Rear J, Salavati R, Stuart K. 2003. Separate insertion and deletion subcomplexes of the *Trypanosoma brucei* RNA editing complex. *Mol Cell* **12:** 307–319. doi:10.1016/S1097-2765(03)00286-7

Schnaufer A, Wu M, Park YJ, Nakai T, Deng J, Proff R, Hol WGJ, Stuart KD. 2010. A protein--protein interaction map of trypanosome ~20S editosomes. *J Biol Chem* **285:** 5282–5295. doi:10.1074/jbc.M109.059378

Sievers F, Wilm A, Dineen D, Gibson TJ, Karplus K, Li W, Lopez R, McWilliam H, Remmert M, Söding J, et al. 2011. Fast, scalable generation of high-quality protein multiple sequence alignments using Clustal Omega. *Mol Syst Biol* **7:** 539. doi:10.1038/msb.2011.75

Sriskanda V, Shuman S. 1998. Mutational analysis of *Chlorella* virus DNA ligase: catalytic roles of domain I and motif VI. *Nucleic Acids Res* **26:** 4618–4625. doi:10.1093/nar/26.20.4618

Stuart KD, Schnaufer A, Ernst NL, Panigrahi AK. 2005. Complex management: RNA editing in trypanosomes. *Trends Biochem Sci* **30:** 97–105. doi:10.1016/j.tibs.2004.12.006

Stuart K, Brun R, Croft S, Fairlamb A, Gürtler RE, McKerrow J, Reed S, Tarleton R. 2008. Kinetoplastids: related protozoan pathogens, different diseases. *J Clin Invest* **118:** 1301–1310. doi:10.1172/JCI33945

Subramanya HS, Doherty AJ, Ashford SR, Wigley DB. 1996. Crystal structure of an ATP-dependent DNA ligase from bacteriophage T7. *Cell* **85:** 607–615. doi:10.1016/S0092-8674(00)81260-X

Unciuleac MC, Goldgur Y, Shuman S. 2019. Structures of ATP-bound DNA ligase D in a closed domain conformation reveal a network of amino acid and metal contacts to the ATP phosphates. *J Biol Chem* **294:** 5094–5104. doi:10.1074/jbc.RA119.007445

Varadi M, Anyango S, Deshpande M, Nair S, Natassia C, Yordanova G, Yuan D, Stroe O, Wood G, Laydon A, et al. 2022. AlphaFold protein structure database: massively expanding the structural coverage of protein-sequence space with high-accuracy models. *Nucleic Acids Res* **50:** D439–D444. doi:10.1093/nar/gkab1061

Worthey EA, Schnaufer A, Mian IS, Stuart K, Salavati R. 2003. Comparative analysis of editosome proteins in trypanosomatids. *Nucleic Acids Res* **31:** 6392–6408. doi:10.1093/nar/gkg870

See the following page for ***Meet the First Author***

MEET THE FIRST AUTHOR

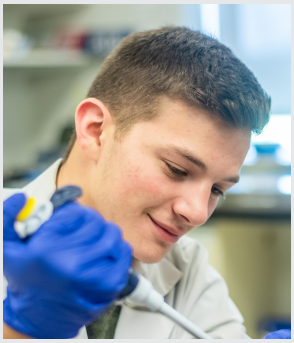

Daniel Moses

***Meet the First Author(s)* is an editorial feature within *RNA*, in which the first author(s) of research-based papers in each issue have the opportunity to introduce themselves and their work to readers of *RNA* and the RNA research community. Daniel Moses is the first author of this paper, "The discovery and characterization of two novel structural motifs on the carboxy-terminal domain of kinetoplastid RNA editing ligases." Daniel is a master's student at the Institute of Parasitology of McGill University. The laboratory investigates the complex biological processes of kinetoplastid parasites, and this article details the structure and mechanism of an essential RNA editing ligase in *Trypanosoma brucei spp*.**

What are the major results described in your paper and how do they impact this branch of the field?

We characterized the structural and functional domains of KREL1 and KREPA2 proteins and investigated their mechanism of dsRNA ligation. We identified two critical regions of the carboxy-terminal domain of KREL1. The first region is the binding site for KREL1's interacting partner KREPA2, and the second region is the KWKE motif VI essential for ATP hydrolysis. This work describes the detailed mechanism unique to this RNA ligase and provides entry points for target-based drug discovery.

What led you to study RNA or this aspect of RNA science?

Biochemistry is the discipline which feeds my scientific interest. Kinetoplastids perform a unique post-transcriptional modification involving the structurally diverged ligase and this process is fascinating! I enjoyed working with proteins and RNA in the laboratory where I was able to apply my theoretical knowledge of biochemistry for practical use. Each new finding led to more curiosity, and new questions continued to evolve.

During the course of these experiments, were there any surprising results or particular difficulties that altered your thinking and subsequent focus?

The oligonucleotide binding fold (OB-fold) domain and zinc finger domains are structurally conserved in numerous protein families. We show that these domains that are present in KREPA2 have no role in KREL1 interaction and have no impact on the activity of KREL1 ligation. Interestingly, this is very different from our human DNA ligase!

What are some of the landmark moments that provoked your interest in science or your development as a scientist?

In science, you are given the tools and resources to investigate the scientific questions you ask. In the laboratory, I asked specific questions about KREL1 and KREPA2 that were previously unknown and then created experiments to answer them. It was a great feeling to obtain concrete data after a rigorous process of optimization and troubleshooting. As an adamant believer in the communication of science, I had the pleasure of presenting this work in different capacities such as poster and oral presentations as well as compiling this work for publication.